Phase Transitions in Monolayers of Human Apolipoprotein C-I

V. M. Bolaños-García and J. Mas-Oliva

Instituto de Fisiología Celular, UNAM, P.O. Box 70-243, México D. F. 04510

S. Ramos and R. Castillo*

Instituto de Física, UNAM, P.O. Box 20−364, México D. F. 01000

Received: November 6, 1998

Human apolipoprotein C-I was deposited onto a highly ionic water subphase to form a monolayer in a Langmuir trough. Pressure−area isotherms of the human apolipoprotein C-I monolayer, as well as direct observations with Brewster angle microscopy, were carried out. Two first-order phase transitions were found. The first phase transition involves the coexistence of a fluid condensed phase and a gas phase, whereas the second one is a transition between two condensed phases. A protein model is proposed, where the apolipoprotein C-I is made of two amphiphilic α-helices bonded with a poorly structured polypeptide fragment. With this model, we have been able to explain our results, in particular the second phase transition, which seems to correspond to a conformational change in the protein. This conformational change could be due to the desorption of one amphiphilic α-helix from the subphase, when lateral pressure is applied to the protein monolayer. The relevance of this conformational change for lipid binding activity is discussed.

1. Introduction

Langmuir monolayers of fatty acids on the surface of water have been studied intensively for decades. However, sensible advances have been obtained only in the past few years as a result of new experimental techniques: X-ray diffraction,[1] polarized fluorescence microscopy,[1] and Brewster angle microscopy.[2,3] These new experimental techniques have revealed that all singularities in the surface pressure−area (Π-*A*) are due to phase changes, each one with a different molecular organization. Bibo et al.[4] have shown that molecular organization of condensed phases in fatty monolayers can be seen as a direct analogue of some specific smectic phases. Thus, each phase can be described in terms of four order parameters. These parameters are (a) positional order; (b) bond or lattice orientational order; (c) tilt order, which is the order of the molecular tilt azimuth with respect to the local orientational order; and (d) herringbone order or broken axial symmetry, which is the staggered ordering of the planes of all-trans hydrocarbon chains. For these order parameters, a distinction has been made between quasi-long-range order, in which the order decays according to a power law, and short-range order, in which the order falls off exponentially with distance. The work of many different groups has contributed to obtaining a general picture of the phase diagram of monolayers of fatty acid as well as the structure of their phases. This can be reviewed as follows:[5] At very low surface densities (a = area/molecule), when the average area per molecule is much larger than the cross-sectional area of an isolated molecule, an amphiphilic monolayer behaves as a two-dimensional gas. Here, a molecule in a monolayer is still free to show all of the conformational entropic contribution without any interference from neighbors. A first-order phase transition from the gas phase to a liquid-expanded (LE) phase is observed upon compression of the monolayer. This phase is isotropic and molecules are tilted, although this tilting is not correlated.[6] The gas-phase side of the transition is of the order of $a = 300-1500$ Å^2/molec. Whereas, on the LE side, a is of the order of the cross section area of an isolated chain (30−40 Å^2). A second phase transition to the liquid-condensed (LC) state is observed upon further compression of the monolayer (a in the order of 22−25 Å^2/molec). Here a is just barely larger than the cross-sectional area of a fully stretched (all-trans) chain. As a matter of fact, condensed phase is made up of a variety of mesophases, i.e., phases where the translational order of the molecules is short-range and the orientational order of the bonds between the molecules is long-range. At low surface pressures, there are several phases showing molecular tilt with distinct symmetry. The phase L_2 has a collective tilt toward a nearest neighbor (NN). The phases L'_2 and Ov (Overbeck) tilt to a next-nearest neighbor (NNN) molecule. At high pressure, there are two untilted phases, the super liquid phase, LS, and the solid phase, S. The structures of these mesophases can be locally hexagonal (LS) or distorted hexagonal, i.e., centered rectangular (L_2, L'_2, Ov, S). In addition to mesophases, crystalline phases also have been found. They are CS and L_2'' phases, which are centered rectangular with herringbone order. L_2'' is a two-dimensional crystal with NN tilt and CS is untilted. At higher pressures, all of the phases collapse in multilayers.

The monolayer's free energy F may be represented as a sum of four terms:[5]

$$F = F_{\text{trans}} + \mathrm{F}_{\text{att}} + \mathrm{F}_{\text{conf}} + \mathrm{F}_{\text{head}}$$

F_{trans} represents the two-dimensional translational entropy of the molecules, including the effects of excluded-area interaction. $F_{\text{trans}} \approx -NkTLn(A\text{-}Nb)$, i.e., van der Waals approximation, where b is the excluded area per molecule and A the area. F_{att} and F_{head} represent the interaction between amphiphilic tails and polar heads, respectively. F_{conf} is a sum of single molecule terms incorporating contributions from internal degrees of freedom

* To whom correspondence should be addressed. E-mail: rolandoc@fenix.ifisicacu.unam.mx.

10.1021/jp984342r CCC: $18.00
Published on Web 07/13/1999

(e.g., internal rotations around tail bonds). One important feature obtained from the case of fatty acid monolayers, to be used in the present study, is related to the difficulty in understanding the two successive fluid−fluid phase transitions. This difficulty relies in identifying the structure of the two phases and the order parameter of the transition between them. The first transition was easy to understand. It is a first-order phase transition (G-LE) which is governed primarily by a tradeoff between F_{trans} and F_{att}, i.e., a loss in translational entropy of the gas phase for a gain in attractive potential energy in the liquid phase. However, for the case of the second first-order phase transition, a direct analogy with liquid crystal systems can lead to a misunderstanding.[5] Rodlike molecules forming liquid crystal systems undergo an isotropic nematic transition in three dimensions without the need for attractive forces between particles. Here, one could think that a discontinuous onset of orientational order appears spontaneously upon compression. Thus, one could expect that the LE−LC transition would be analogous to the isotropic−nematic transition in liquid crystals. However, if the observed molecules are treated as rigid rods (grafted rods) that interact through their excluded volumes, it can be shown that the increase in orientational order under compression is continuous.[7,8] Several works on this issue have provided a general picture.[5,9] Here, when the monolayer is further compressed the molecules must stretch out (if they are flexible) and/or desorb some of their segments from the surface and stand upright, so as to occupy less surface area. This transition may be of first-order if, following the conformational change, the molecules can get considerably close to each other, thus increasing the number of interchain interactions; i.e., this transition is governed primarily by an interplay between F_{conf} and F_{att}.

Several studies have been carried out in protein monolayers. Horse muscle cytochrome-*c* deposited on a stearic acid monolayer has been studied by Tanaka et al.[10−12] These authors studied the films with pressure−area isotherms and made observations with fluorescence microscopy and Brewster angle microscopy. However, they did not recognize the role of phase transitions in their binary mixture monolayers. The same occurs in the case of acetylcholinesterase studied with Brewster angle microscopy and atomic force microscopy,[13] where the authors only reported the formation of domains when the monolayer is compressed. Frey et al.[14] have followed a two-dimensional crystallization of streptavidin using a Brewster angle microscope (BAM) with great success. Lipp et al.[15] studied, with fluorescence microscopy, polarized fluorescence microscopy, and Brewster angle microscopy, how the human lung surfactant protein SP-B and its amino terminus ($SP\text{-}B_{1-25}$) alter the phase behavior of palmitic acid monolayer. They observed how the protein inhibited the formation of condensed phases of palmitic acid and the formation of a new fluid protein-rich phase. Recently, Chen et al.[16] studied the molecular orientation of tetra-α-helical heme proteins $(\alpha ss\alpha)_2$ in monolayer and Langmuir−Blodgett films. They obtained pressure−area isotherms with at least two phase transitions. However, the lack of a direct observation of the monolayers misled the authors in the proper assignation of the phases, since liquid-expanded−gas transition usually occurs at very low surface pressure values, and, in contrast, transitions between condensed phases take place at a higher surface pressure.

The human apolipoprotein C-I (APO C-I) is a plasma protein of 57 amino acid residues in length. This protein plays a key role in the quilomicron uptake[17] and in the regulation of apolipoprotein-E/β-VLDL (very low-density lipoproteins) particle interaction.[18] The structure−function relationship of human apolipoproteins, including APO C-I, is not well understood because of a lack of information about the way that the different protein conformations are related to lipid binding activity. Two crystalline forms of APO C-I have been reported as suitable for high-resolution X-ray diffraction analysis.[19] However, their three-dimensional structures still remain unsolved. On the other hand, studies based on nuclear magnetic resonance and circular dichroism spectroscopy have demonstrated that synthetic peptides corresponding to residues 1−38 (sequence TPDVSSALDKLKEFGNTLEDKARELISRIK),[20] 7−24 (sequence ALDKLKEFGNTLEDKARE),[21] and 35−53 (sequence SAKMREWFSETFQKVKEKL)[22] show the amphiphilic α-helix motif as their main secondary structure. Other human apolipoproteins, including AI, AII, CII, CIII, and E, present no similarities on the basis of their primary structure.[23,24] Nevertheless, when they are compared at a secondary structure level, as well as in their common lipid binding activity, important similarities appear among them, mainly owing to the presence of amphiphilic α-helices. These structures might correspond to the lipid-associating domains, as previously reported by our group.[23,25]

The aim of this paper is to present a study about the properties of the human APO C-I monolayer. Here, we present the pressure−area isotherm of this monolayer, together with direct observations using Brewster angle microscopy. This study gives a new physical insight into the APO C-I structure and the way lipid binding activity could occur.

2. Experimental

Lyophilized human APO C-I (99%, PerImmune Incorporation) solubilized in a buffered solution (pH = 8.0), was filtered with a 0.22 μm membrane filter and spread onto a subphase of a phosphate buffered solution of 3.5M KCl (Baker, Mexico) prepared with ultrapure water (Nanopure-UV). The buffer added to the subphase was prepared with sodium phosphate at a concentration of 20 mM and pH = 8.0. It is important to note that before preparing these solutions, the KCl salt was heated for 4 hours at 300 °C to prevent spurious organic compounds in the subphase. The monolayers were prepared on a computerized Nima Langmuir−Blodgett trough (TKB 2410A, Nima Technology Ltd., England) using a Wilhelmy plate to measure the surface pressure, $\Pi = \gamma_o - \gamma$, i.e., the surface tension difference of the clean subphase and that of the protein covered subphase. The trough was isolated from vibrations using a pneumatic tube incorporated into a steel base. The barriers are made of PTFE fitted with stiffening bars defining a working circular area, starting at 1000 cm^2. All experiments were carried out in a dust-free environment. The speed of compression was in the order of 40 cm^2/min (441 $Å^2$/molec min).

The protein concentration of the solution to be spread was determined according to the equation $A = \epsilon lC$. Here, A is the sample absorbance, l is the path length, ϵ is the molar absorption coefficient, and C is the protein concentration. The molar absorption coefficient was estimated by two methods. In the first one, ϵ was obtained experimentally from UV absorbance measurements. APO C-I was dialyzed against water, then lyophilized and weighted in an analytical scale. Afterward, the determination of maximum absorption in the UV region was carried out. The maximum absorption was found at 278 nm and the ϵ value was obtained; $\epsilon = 5640\ cm^{-1}\ M^{-1}$. In the second method, ϵ was calculated with the equation proposed by Pace et al.[26]: $\epsilon_{(280\ nm)} = 5500W + 1490Y + 125C$ where W, C, and Y are the number of tryptophan, tyrosine, and cysteine amino acid residues, respectively. In this case we obtained $\epsilon = 5500\ cm^{-1}\ M^{-1}$. The final ϵ value was determined using an average

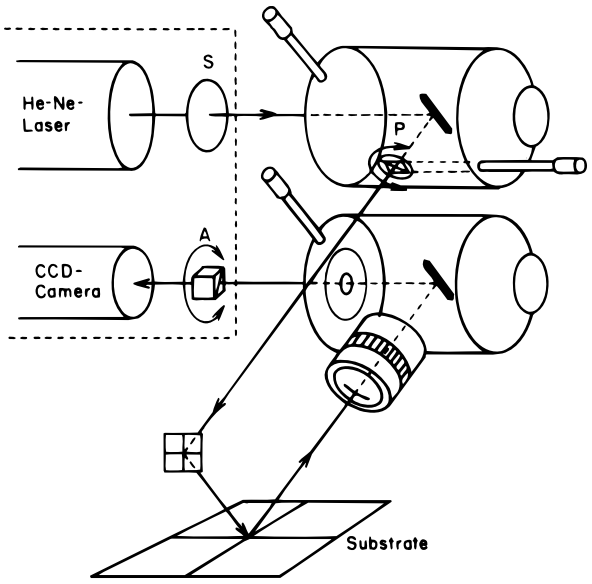

Figure 1. A diagram of a Brewster angle microscope.

coming from both methods; $\epsilon_{average} = 5570\ cm^{-1}\ M^{-1}$. The concentration of the protein solution used in our studies was 0.2 mg/mL.

Far-UV circular dichroism spectra of the protein solution was recorded on a spectropolarimeter (Aviv 62DS, Aviv Associates Inc., NJ) in a 0.1 cm quartz cell, using an average time of 0.3 s and a step size of 0.5 nm at 20 °C. The α-helix content was calculated using the program PROSEC 3.1 (Aviv Associates Inc., NJ). The signal dependence on protein concentration was calculated using several samples, with concentrations ranging between 100 μg/mL and 250 μg/mL.

A secondary structure prediction for the APO C-I was obtained with a program based on the Profile Network Prediction Heidelberg method (PHD version 5.94-317, Heidelberg). This method uses a neural network approach averaging several independently trained networks before making a final prediction. The final prediction has a reliability above 72%.[27]

Brewster angle microscopy[2,3] is a relatively new technique that allows direct observation of the films onto the water/air surface during the compression of the monolayer. This is a technique based on the study of the reflected light coming from an interface illuminated at the Brewster angle by a laser beam polarized in the plane of incidence. When the angle of incidence of the laser beam is the Brewster angle, there is no light reflected from a clean and perfect interface, i.e., the refractive index changes abruptly from one medium to another. For a real interface which has a transition region where the refractive index changes smoothly from one value to another, the reflected intensity at the Brewster angle is a minimum, but it does not vanish completely. The reflected intensity depends strongly on the interfacial characteristics, such as molecular density and molecular anisotropy. These properties are particularly modified when a monolayer is located at the interface. Thus, a monolayer on an interface is able to produce reflection of light. In tilted phases, the anisotropy is sufficiently strong to have enough light reflection to make quite visible the mosaic of textures due to tilted domains. In untilted phases with rectangular lattice symmetry, textures are also visible, but with much less contrast. Phase transitions are visible either as a dramatic change in the degree of contrast or as a sudden alteration of the mosaic of textures and domain borders. Figure 1 shows a BAM in a schematic way. The interface is illuminated at the Brewster incidence (∼53°) with a polarized laser beam from a He−Ne laser. A microscope receives the reflected beam that is analyzed by a polarization analyzer. The signal is received by a CCD video camera to develop an image of the monolayer.

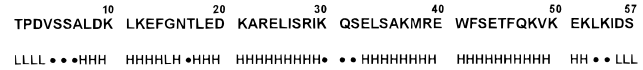

Figure 2. The secondary structure prediction for APO C-I. This protein forms two α-helices separated by a poorly structured region according to the PHD method. H = α-helix, L = loop, and ● = no prediction is made for these amino acid residues.

BAM observations were performed in a BAM1 Plus (Nanofilm Technologie GmbH, Germany), with a spatial resolution ca. 4 μm. The BAM analyzer gave the best contrast while kept at 0° or 180°. The Nima LB trough and the BAM are placed on concrete tables cemented to a concrete floor on the ground floor of our building. Temperature in the trough was kept constant with the aid of a water circulator bath (Cole-Parmer 1268-24).

Results and Discussion

The secondary structure prediction for the APO C-I obtained with the Profile Network Prediction Heidelberg program is shown in Figure 2. Here, the APO C-I prediction gives a high α-helix content, distributed in two α-helices encompassing the residues 8−29 and 33−52 separated by a short, poorly structured region. Such a prediction is in good agreement with the amphiphilic α-helical regions proposed by Rozek et al.[20−22] These regions encompass the amino acid residues 4−30 and 35−53. The first α-helix (4−30) presents approximately 7.5 periods and the second one (35−53) 5.2 (1 period = 3.6 amino acids). The amino acid residue distributions for these amphiphilic α-helices are shown as helical-wheel projections in Figure 3. On the basis of these images, the amino acid residues 4−30 and 35−53 present charged amino acid residues clustered at the polar protein faces, whereas, a hydrophobic surface is formed at the opposite faces of these α-helices. Therefore, this protein has an amphiphilic character due to the uneven polar/nonpolar amino acid residue distribution. In addition, on the basis of the amphiphilic α-helix classification of Jones et al.[28] and the amino acid residue distributions shown in the helical wheels, the amphiphilic α-helices of human APO C-I were classified by us as belonging to class A. This class of amphiphilic α-helices is commonly found in apolipoproteins.[23−25] The most distinctive feature of the amphiphilic α-helices of class A is their unique clustering of positively charged residues at the polar/nonpolar interface and of the negatively charged amino acid residues at the center of the polar face. Affinity of amphiphilic α-helices of class A for water/air interfaces is influenced by several physicochemical properties. The most relevant are the hydrophobicity of the amino acid side chains on the nonpolar face of the α-helix, the number and distribution of charged residues around the α-helix axis, the magnitude of the hydrophobic moment (μH), and the length of the α-helix.[29] Furthermore, amphiphilic α-helices of class A are subdivided into two subclasses: A1 and A2. The differences mainly reside in the higher lysine/arginine ratio and higher μH values for the proteins in the A2 subclass. The specific charge clustering in amphiphilic α-helices of class A2 could be important for initial lipid−apolipoprotein association because of electrostatic interactions, as observed for human lipid binding proteins such as APO C-I.[30]

An estimation of the hydrophobic moment[31] for the amphiphilic α-helices of APO C-I was made with the PCGene Program (Helixmem, IntelliGenetics Inc., 1991)[32] using the following expression:

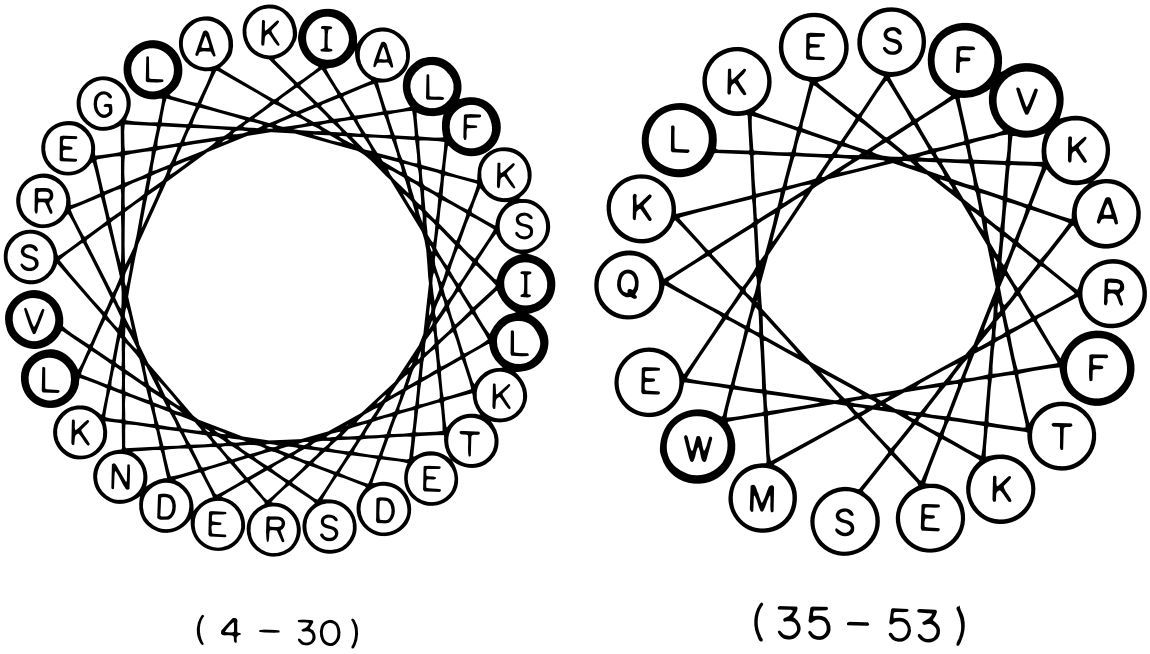

Figure 3. Helical wheel projections of the amphiphilic α-helices present in APO C-I. The numbers between parentheses indicate the encompassed amino acid residues.

$$\mu\mathrm{H} = \frac{1}{N}\sqrt{[\sum_{n=1}^{N} H_n \sin(\delta n)]^2 + [\sum_{n=1}^{N} H_n \cos(\delta n)]^2}$$

where, H_n is the numerical hydrophobicity of the nth residue. These hydrophobicity values are related to the free energy of transfer of the amino acids from the inside to the surface of a globular protein,[33] and they depend slightly on the hydrophobicity scale used.[32] Here, δ corresponds to the angle formed between amino acid lateral chains of two adjacent residues with respect to the plane of the α-helix (for an ideal α-helix, $\delta = 100°$). α-Helical regions with μH values higher than 0.2 kcal/mol per residue could be considered as good amphiphilic α-helices.[28] Our calculation for APO C-I (4−30) gives μH= 0.54 kcal/mol per residue, and for APO C-I (35−53) located near the carboxy terminus region of the protein, gives μH = 0.36 kcal/mol per residue. Consequently, the amino end of APO C-I (4−30) could interact in a stronger fashion with the water−air interface than the carboxy terminus region (35−53). This can be due to two reasons: (a) the high value of μH for APO C-I (4−30) with respect to the μH value for APO C-I (35−53) and (b) the length of the APO C-I (4−30), which is longer than the APO C-I (35−53).

The CD analysis carried out for the protein is shown in Figure 4. The far-UV CD spectrum of APO C-I is consistent with a well-preserved α-helix structure. We found a maximum ellipticity at 195 nm and a double minimum at 208 and 222 nm. This measurement ensures the integrity of the APO C-I protein prior to the monolayer preparation.

Although apolipoproteins are soluble in water, they are insoluble in subphases that contain a high salt concentration and remain at the interface when spread directly onto a 3.5 M KCl subphase solution.[34] This fact indicates that a monolayer of this kind of proteins will behave as a Langmuir monolayer, where the protein is not dissolved in the subphase. Figure 5 shows a typical isotherm for APO C-I protein monolayer in a buffered subphase with a high content of KCl, at 25.1 °C. Several features are clearly seen in the isotherm: (a) A region of $\Pi \sim 0$ mN/m, starting at very low surface area density, whose

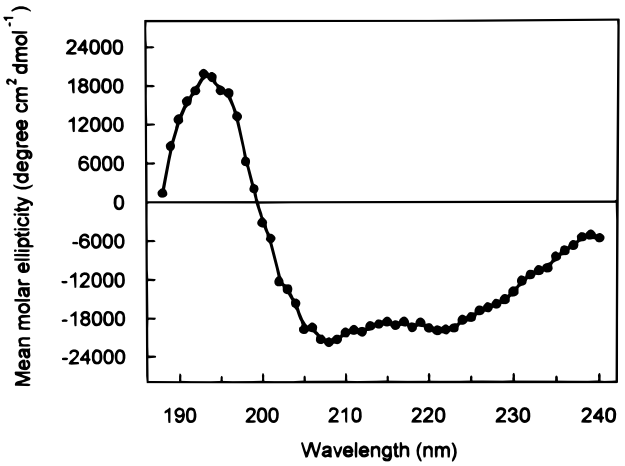

Figure 4. Far-ultraviolet circular dichroism of the human APO C-I protein.

ending is of the order of $a = 5500$ Å^2/molec. This behavior is reminiscent of a gas/condensed transition, which will be confirmed below. (b) Afterward, there is an important increase in the pressure similar to the case of condensed phases. This phase is compressed until we find a big kink at $\Pi \sim 37$ mN/m and $a = 1000-1250$ Å^2/molec. This feature is typical of a phase transition, which is confirmed with BAM observations, as shown below. The range between the two ends of the coexistence is in the order of $a = 200-250$ Å^2/molec. The phases involved in this transition are condensed phases due to the relatively high incompressibility of the monolayer there. (c) At the end of the compression, the collapse is reached at a Π ca. 47 mN/m and $a \sim 550$ Å^2/molec. It is important to mention here, that a phase transition between two condensed phases is not commonly found in proteins.

BAM observations were done along the compression of the protein monolayer. The gas/condensed phase coexistence was confirmed when we started our compression at low Π and low area density. The condensed domains are so large that it is not easy to see areas with gas phase at densities of the order of 6000 Å^2/molec. Figure 6a shows an image close to the end of

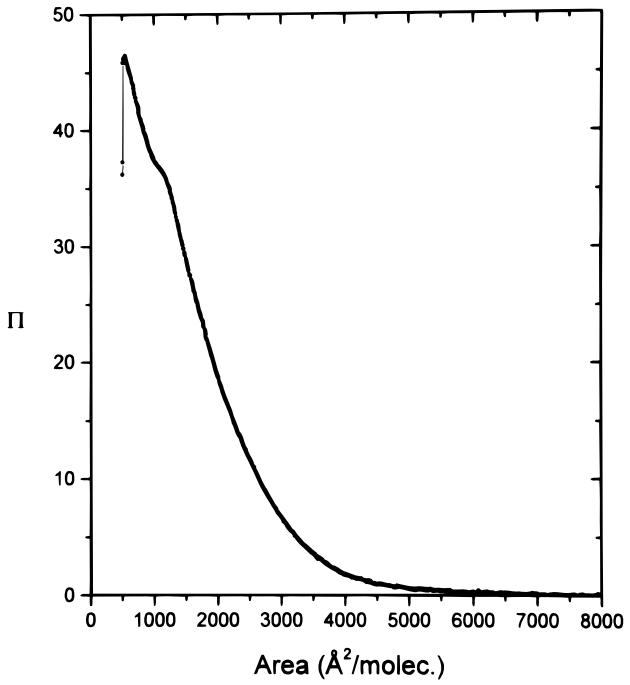

Figure 5. Typical Π vs *a* isotherm for human APO C-I at 25.1 °C. Π is in mN/m.

the gas/condensed phase coexistence ($a \sim 5500$ Å^2/molec), at the condensed phase side. Here, we can see bright condensed-phase domains and dark areas of gas phase. The bright domains are moving, as it is common in this kind of coexistence because of the low viscosity of the gas phase. After the end of the coexistence, no gas phase remains and no domains with different shades of gray are observed. When the second transition is reached in the Π-a isotherm, big elongated domains appear in the field of view of the BAM, as shown in Figure 6b−e. These domains are bright, i.e., with high reflectivity. At the start of this coexistence, it is clear that the condensed phase previously found was quite fluid. Close to the borders of the big bright domains, it is easy to see streams of fluid flowing. For this reason, we have named the first condensed phase as liquid (L) phase and the second condensed phase as liquid condensed (LC) phase. In some cases, the elongated LC domains are greater than the field of view of the BAM (∼800 μm) and quite curly. In our images at the L/LC coexistence, besides these elongated domains and L phase, there are many very small domains of LC phase that appear like a spotted area, since they are not in focus. The elongated domains never showed facets or different shades of gray. After the L/LC coexistence, we compressed the LC phase, and before the collapse is reached, a lot of defects (Newton rings) appeared. This is explained because healing between domains is not easily achieved in this phase. At the collapse point, we see too many defects that cannot be focused. For instance, we can identify Newton rings and multilayer domains as white grains and mountain shaped structures (Figure 6f).

Several BAM observations were made along the L/LC phase transition, through compression−expansion cycles. We used several compression speeds and waiting times between the cycles. In some cases, we did not actually expand the system to go from the LC phase to the L phase; rather, we just left the system relaxing. On expansion, when the L phase is reached all of the LC domains completely disappeared from the field of view of the BAM. There is no contrast in the BAM images at this moment, since we are in the L phase. However, when the LC phase is reached again on compression, the domains reformed with the same shape but larger. We observed hysteresis in the starting of the phase transition, as well as the enlargement of domains. The domains in the first compression cycles were not so large as in the last cycles. BAM observations, as shown before, revealed that the transition was not continuous. Therefore, on the basis of these facts, we classified the L/LC phase transition as a first-order transition.

On the basis of our results, it is reasonable to model the APO C-I protein as two amphiphilic α-helices bonded by a loose hinge. This protein would be traveling in a landscape of close energy minimum configurations when deposited onto a water subphase, which is also working as a thermal reservoir. The different protein configurations must have the restriction of laying horizontally on the subphase (Figure 7a), because of the amphiphilic character of the protein. At low surface area, two phases are coexisting. BAM observations showed that in both phases, there is only one kind of shade; dark in the G phase and gray in the L phase. There are no monolayer domains revealing molecular order, which could give different textures, i.e., they are disordered phases. The G/LE first-order phase transition is probably governed mainly by a tradeoff between F_{trans} and F_{att}, i.e., a loss in translational entropy of the gas phase for a gain in attractive potential energy in the liquid phase.

The understanding of the second phase transition in the monolayer would give a physical insight about the behavior of the protein. Here, it is necessary to explain the leap in area per molecule and the origin of the bright domains that appeared in the BAM observations along the phase transition. The leap area per molecule along the transition is in the order of 200−250 Å^2/molec, i.e., slightly less than half of the collapse area (550 Å^2/molec). In our model, each amphiphilic α-helix could be considered as a long cylinder partially embedded in the water subphase. An estimation of the projected area of each embedded cylinder on the subphase gives ca. 200 Å^2 for the (4−30) α-helix and ca. 140 Å^2 for the (35−53) α-helix. On the other hand, the high contrast between L and LC domains, as observed with the BAM during the phase transition, could be explained as thinking that a part of the protein molecule is getting out of the surface. This proposal also could explain the leap in surface density along the transition. This behavior is similar to the case of a second transition in fatty acids. When a fatty acid monolayer is compressed, the molecules must change their conformation and stretch out after the first G/L transition. This could be the case in the APO C-I protein monolayer. The protein molecule could desorb one of its amphiphilic α-helical segments from the surface to occupy less surface area. This conformational change could explain the area loss and the high reflectivity difference between the phases. In addition, the desorbed α-helices are correlated neither intra- nor supramolecularly, because different textures are not observed in the domains of the LC phase. The amphiphilic α-helical segment going out from the surface would be the smaller one (35−53), because of its low μH value and short size, as mentioned above (Figure 7b). Therefore, the L/C transition seems to be of first order, because of the large change of area per molecule. After the conformational change, protein molecules are considerably close to each other, surely increasing the attractive contribution to the free energy. The transition must be governed primarily by an interplay between F_{conf} and F_{att}.

At this stage it is important to note that the amphiphilic α-helices show good stability in water/lipid, water/air interfaces.[35,36] A good example is APO C-I that in physiological conditions stays bound to the surface of a lipoprotein in the plasma. Moreover, alamethicin, a membrane peptide of 20 amino acids, when placed in an interface, shows a characteristic α-helix

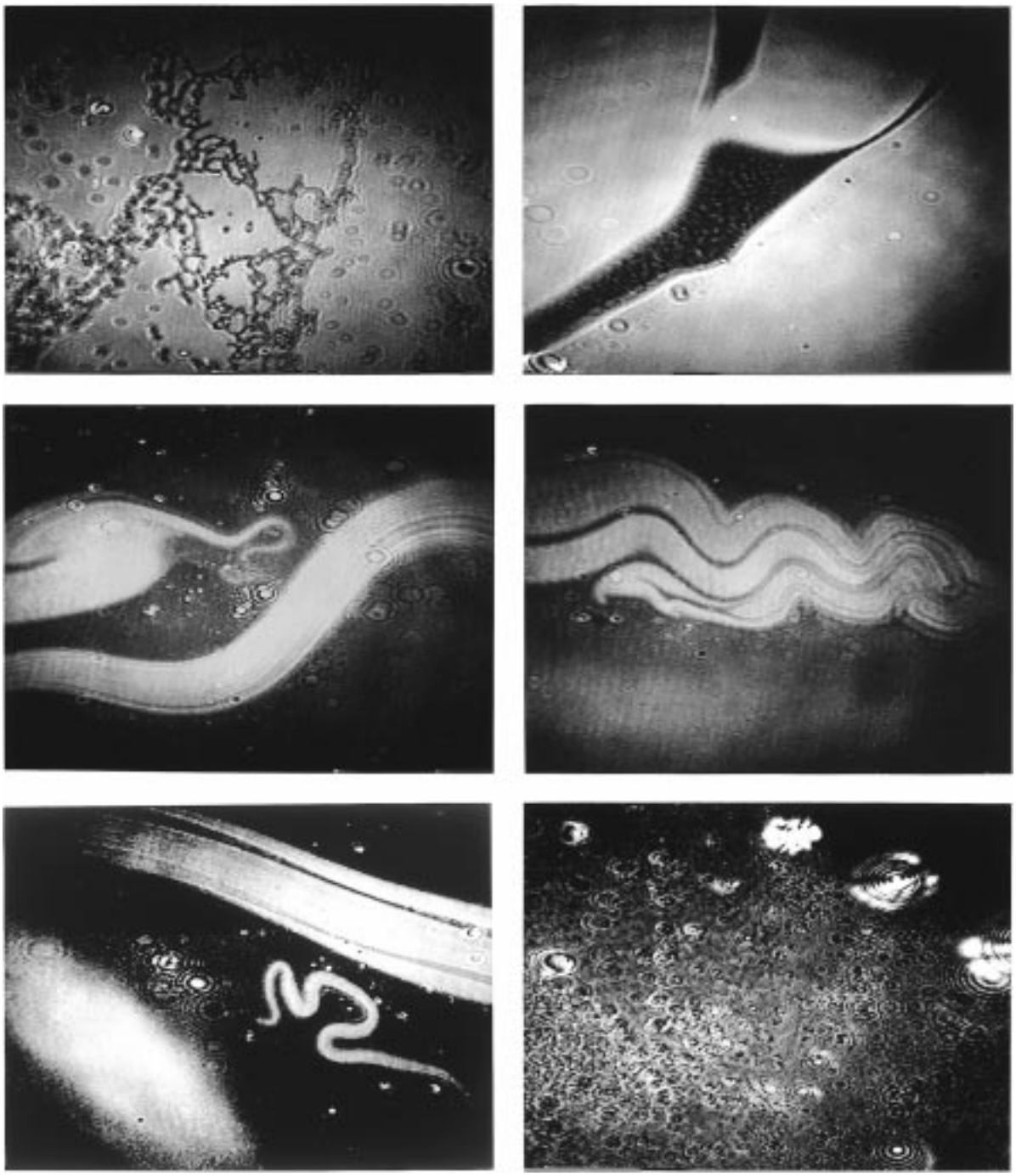

Figure 6. Brewster observations of the human APO C-I protein monolayer: (a) gas/liquid coexistence, $\Pi \sim 0$ and $a = 6500$ Å^2/molec; (b−e) different observations at the L/CL coexistence $\Pi \sim 37$ mN/m and $a \sim 1200$ Å^2/molec; (f) collapsed monolayer $\Pi \sim 47$ and $a \sim 550$ Å^2/molec.

circular dichroism spectrum at low relative humidity, whereas, it is lost at 100% relative humidity.[37] Since hydration of the α-helix backbone is an important factor in unfolding α-helices, it has been demonstrated that the phenomenon is highly residue-specific.[38,39] Molecular dynamics proposes that side chains forming intramolecular hydrogen bonds with the backbone stabilize α-helices in a vacuum where water would tend to unfold the α-helix.[39] These arguments would support the fact that the shorter APO C-I might move upward in a fairly stable fashion rather than downward, where, owing to the high salt concentration of the interface, this α-helix most probably would unfold.

The conformational specificity of APO C-I is most probably imposed through a postulated stereochemical code[40] that in turn arises from the interplay between the shape and polarity of residue side chains and secondary structure. In this way, a simple binary pattern of polar and nonpolar residues along the polypeptide chain favor the formation of amphiphilic α-helices, that in turn might be important in the way the polypeptide chain interacts with the lipid particle.

The desorption phenomenon observed in our investigation might be involved in the way APO C-I (an example of exchangeable apolipoproteins) initiates the process of displacement from lipoprotein particles, where a portion of the molecule separates from the donor particle first, to be accepted by an acceptor particle as the following step. The way these exchangeable apolipoprotein molecules move between lipoprotein particles has remained as an open question. On the basis of our observations, we propose, for the first time, a possible mechanism to explain the initial movement of APO C-I. This

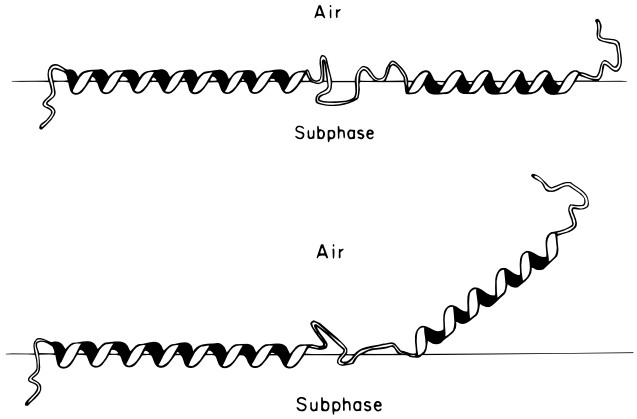

Figure 7. Proposed model for the human APO C-I: (a) protein laying over the subphase at low pressures and (b) protein laying over the subphase with the amphiphilic α-helical segment (35−53) going out from the surface, when pressure reaches the L/LC phase transition.

mechanism is based on the desorption from the surface of one of the α-helices, when lateral tension in a given lipoprotein particle could build up because of changes in its volume and/or shape, as well as by the presence of other apolipoproteins in the same lipoprotein particle. Our results indicate that the basic physicochemical characteristics of APO C-I dictate the major conformational changes found upon self-association of APO C-I, which in turn would directly affect its affinity for lipids.

Acknowledgment. The support from CONACYT (27513-E) and DGAPA-UNAM (IN103598 and IN215397) is gratefully acknowledged.

References and Notes

(1) Knobler, C. M. In *Advances in Chemical Physics*, LXXVII; Prigogine, I., Rice, S. A., Eds.; Wiley: New York, 1990; p 397.
(2) Höning, D.; Möbius, D. *J. Phys. Chem.* **1991**, *95*, 4590.
(3) Henon, S.; Meunier, J. *Rev. Sci. Instrum.* **1991**, *62*, 936.
(4) Bibo, A. M.; Knobler, C. M.; Peterson, I. R. *J. Phys. Chem.* **1991**, *95*, 5591.
(5) Andelman, D.; Brochard, F.; Knobler, C. M.; Rondelez, F. In *Micelles, Membranes, Microemulsions, and Monolayers*; Gelbart, W. M., Ben-Sahul, A., Roux, D., Eds.; Springer: New York, 1994; Chapter 12.
(6) Rasing, Th.; Shen, Y. R.; Kim, M. W.; Grubb, S. *Phys. Rev. Lett.* **1985**, *55*, 2903.
(7) Chen, Z. Y.; Talbot, J.; Gelbart, W. M.; Ben-Shaul, A. *Phys. Rev. Lett.* **1988**, *61*, 1376.
(8) Halperin, A.; Alexander, S.; Schechter, I. *J. Chem. Phys.* **1987**, *86*, 6550.
(9) Kramer, D.; Ben-Shaul, A.; Chen, Z. Y.; Gelbart, W. M. *J. Chem. Phys.* **1992**, *96*, 2236.
(10) Tanaka, H.; Akatsuka, T.; Murakami, T.; Ogoma, Y.; Abe, K.; Kondo, Y. *J. Biochem.* **1997**, *121*, 206.
(11) Tanaka, H.; Akatsuka, T.; Ohe, T.; Ogoma, Y.; Abe, K.; Kondo, Y. *Polym. Adv. Technol.* **1998**, *9*, 150.
(12) Tanaka, H.; Hayashi, K.; Akatsuka, T.; Murakami, T.; Toyama, J.; Noda, K.; Kida, T.; Ogoma, Y.; Fujii, T.; Kondo, Y. *J. Biochem.* **1995**, *117*, 1151.
(13) Dziri, L.; Boussaad, S.; Wang, S.; Leblanc, R. M. *J. Phys. Chem. B* **1997**, *101*, 6741.
(14) Frey, W.; Schief, W. R.; Vogel, V. *Langmuir* **1996**, *12*, 1312.
(15) Lipp, M.; Lee, K. Y. C.; Waring, A.; Zasadzinki, J. A. *Biophys. J.* **1997**, *72*, 2783.
(16) Chen, X.; Moser, C. C.; Pillud, D. L.; Dutton, P. L. *J. Phys. Chem. B* **1998**, *102*, 6425.
(17) Eisenberg, S. *Curr. Opin. Lipidol.* **1990**, *1*, 205.
(18) Swaney, J. B.; Weisgraber, K. H. *J. Lipid Res.* **1994**, *35*, 134.
(19) Weisgraber, K. H.; Newhouse, Y. M.; McPherson, A. *J. Mol. Biol.* **1994**, *236*, 382.
(20) Rozek, A.; Buchko G. W.; Kanda, P.; Cushley, R. J. *Protein Sci.* **1997**, *6*, 1858.
(21) Rozek, A.; Buchko, G. W.; Cushley, R. J. *Biochemistry* **1995**, *34*, 7401−7408.
(22) Buchko, G. W.; Rozek, A.; Zhong, Q.; Cushley, R. J. *Peptide Res.* **1995**, *8*, 86.
(23) Bolaños-Garcia, V. M.; Soriano-Garcia, M.; Mas-Oliva, J. *Mol. Cell. Biochem.* **1997**, *175*, 1.
(24) Weinberg, R. B. *J. Lipid Res.* **1994**, *35*, 2212.
(25) Bolaños-Garcia, V. M. 1997, Ph.D. Thesis, National University of México, México.
(26) Pace, C. N.; Vajdos, F.; Fee, L.; Grimsley, G.; Gray, T. *Prot. Sci.* **1995**, *4*, 2411.
(27) Rost, B.; Sander, C. *Proteins* **1994**, *19*, 55.
(28) Jones, M. K.; Anantharamaiah, G. M.; Segrest, J. P. *J. Lipid Res.* **1992**, *33*, 287.
(29) Bolaños-Garcia, V. M.; Soriano-Garcia, M.; Mas-Oliva, J. *Biochim. Biophys. Acta* **1998**, *1384*, 7.
(30) Gazzara, J. A.; Phillips, M. C.; Lund-Katz, S.; Palgunachari, M. N.; Segrest, J. P.; Anantharamaiah, G. M.; Snow, J. W. *J. Lipid Res.* **1997**, *38*, 2134.
(31) Eisenberg, D.; Weiss, R. M.; Terwilliger, T. C. *Nature* **1982**, *299*, 371.
(32) Eisenberg, D.; Schwarz, E.; Komaromy, M.; Wall, R. *J. Mol. Biol.* **1984**, *179*, 125.
(33) Janin, J. *Nature* **1979**, *277*, 491.
(34) Krebs, K. E.; Ibdah, J. A.; Phillips, M. C. *Biochim. Biopys. Acta* **1988**, *959*, 229.
(35) Karle, I. L. *Biopolymers* **1996**, *40*, 157.
(36) Sato, A.; Furuno, T.; Toyoshima, C.; Sasabe, H. *Biochim. Biophys. Acta* **1993**, *1162*, 54.
(37) Wu, Y.; Huang, H. W.; Olah, G. A. *Biophys. J.* **1990**, *57*, 797.
(38) Jayasinghe, S.; Barranger-Mathys, M.; Ellena, J. F.; Franklin, C.; Cafiso, D. S. *Biophys. J.* **1998**, *74*, 3023.
(39) Doruker, P.; Bahar, I. *Biophys. J.* **1997**, *72*, 2445.
(40) Lattman, E. E.; Rose, G. D. *Proc. Natl. Acad. Sci. U.S.A.* **1993**, *90*, 439.